LDA measurements of coherent flow structures and cross-flow across the gap of a compound channel with two half-rods

Bertocchi, F.; Rohde, M.; Kloosterman, J. L.

DOI
10.1016/j.nucengdes.2017.10.023

Publication date
2018

Document Version
Final published version

Published in
Nuclear Engineering and Design

Nuclear Engineering and Design 326 (2018) 17–30

Contents lists available at ScienceDirect

Nuclear Engineering and Design

journal homepage: www.elsevier.com/locate/nucengdes

LDA measurements of coherent flow structures and cross-flow across the gap of a compound channel with two half-rods

F. Bertocchi*, M. Rohde, J.L. Kloosterman

Radiation Science and Technology, Department of Radiation Science and Technology, Delft University of Technology, Mekelweg 15, Delft 2629 JB, Netherlands

ARTICLE INFO

Keywords:
Coherent structures
Rod bundle
Cross-flow
Laser Doppler Anemometry

ABSTRACT

The enhancement of heat transfer from fuel rods to coolant of a Liquid Metal Fast Reactor (LMFR) decreases the fuel temperature and, thus, improves the safety margin of the reactor. One of the mechanisms that increases heat transfer consists of large coherent structures that can occur across the gap between adjacent rods. This work investigates the flow between two curved surfaces, representing the gap between two adjacent fuel rods. The aim is to investigate the presence of the aforementioned structures and to provide, as partners in the EU SESAME project, an experimental benchmark for numerical validation to reproduce the thermal hydraulics of Gen-IV LMFRs. The work investigates also the applicability of Fluorinated Ethylene Propylene (FEP) as Refractive Index Matching (RIM) material for optical measurements.

The experiments are conducted on two half-rods of 15 mm diameter opposing each other inside a Perspex box with Laser Doppler Anemometry (LDA). Different channel Reynolds numbers between Re = 600 and Re = 30,000 are considered for each P/D (pitch-to-diameter ratio).

For high Re, the stream wise velocity root mean square v_{rms} between the two half rods is higher near the walls, similar to common channel flow. As Re decreases, however, an additional central peak in v_{rms} appears at the gap centre, away from the walls. The peak becomes clearer at lower P/D ratios and it also occurs at higher flow rates. Periodical behaviour of the span wise velocity across the gap is revealed by the frequency spectrum and the frequency varies with P/D and decreases with Re. The study of the stream wise velocity component reveals that the structures become longer with decreasing Re. As Re increases, these structures are carried along the flow closer to the gap centre, whereas at low flow rates they are spread over a wider region. This becomes even clearer with smaller gaps.

1. Introduction

The rod bundle geometry characterises the core of LMFBR, PWR, BWR or CANDU reactors, as well as the steam generators employed in the nuclear industry. In the presence of an axial flow of a coolant, this geometry leads to velocity differences between the low-speed region of the gap between two rods and the high-speed region of the main sub-channels. The shear between these two regions can cause streaks of vortices carried by the stream. Generally those vortices (or structures) develop on either sides of the gap between two rods, forming the so-called *gap vortex streets* (Tavoularis, 2011). The vortices forming these *streets* are stable along the flow, contrary to free mixing layer conditions where they decay in time. Hence the adjective *coherent*. The formation mechanism of the gap vortex streets is analogous to the Kelvin-Helmholtz instability between two parallel layers of fluid with distinct velocities (Meyer, 2010). The stream-wise velocity profile must have an inflection point for these structures to occur, as stated in the Rayleigh's instability criterion (Rayleigh, 1879).

Moreover, a transversal flow of coherent structures across the gap between two rods can also occur. In a nuclear reactor cross-flow is important as it enhances the heat exchange between the nuclear fuel and the coolant. As a result, the fuel temperature decreases improving the safety performance of the reactor.

Much research has been done in studying periodic coherent structures and gap instability phenomena in rod bundles resembling the core of LMFBRs, PWRs, BWRs and CANDUs. Rowe et al. (1974) measured coherent flow structures moving across a gap characterised by a P/D of 1.125 and 1.25. A static pressure instability mechanism was proposed by Rehme to explain the formation of coherent structures (Rehme, 1987). Möller measured the air flow in a rectangular channel with 4 rods (Möller, 1991). The rate at which the flow structures were passing increased with the gap size. The instantaneous differences in velocity and vorticity near the gap, responsible of the cross-flow, were associated with a state of *metastable equilibrium*. Recently, Choueiri gave an analogous explanation for the onset of the gap vortex streets (Choueiri

* Corresponding author.
E-mail address: F.Bertocchi@tudelft.nl (F. Bertocchi).

http://dx.doi.org/10.1016/j.nucengdes.2017.10.023
Received 2 June 2017; Received in revised form 14 October 2017; Accepted 25 October 2017

Nomenclature

Latin symbol

A	Flow area, mm^2
$D_{H,GAP}$	Gap hydraulic diameter, m
d_0	Laser beam diameter, mm
f	Flow structure frequency, Hz
H, L	Test section side dimensions, mm
$\mathscr{L}$	Flow structure length, m
l	LDA probe length, mm
N_s	Number of collected samples, –
P/D	Pitch-to-diameter ratio, –
R_i	Inner half-rod diameter, mm
R_{rod}	Half-rod diameter, mm
S	Frequency spectrum, s
t	thickness, mm
$\overline{U}$,U_{rms}	Mean and rms generic velocity, m/s
u^*	friction velocity, m/s
$\dot{V}$	Flow rate, l/s
v	Stream-wise velocity component, m/s
W	Rod-to-rod distance, mm
X, Z	Span-wise and normal-to-the-gap coordinates, mm
z^+	Non dimensional wall distance, –

Non dimensional number

Re	Reynolds
Str	Strouhal

Greek symbol

α	Laser half beam angle in air, °
β	Laser half beam angle through Perspex, °
γ	Laser half beam angle in water, °
η	Refractive index, –
λ	Laser wavelength, nm
μ	Dynamic viscosity, Pa·s
ρ	Density, kg/m^3
σ	Standard deviation around the mean frequency, Hz
ε_m,ε_{rms}	95% conf. interval for mean and rms values, –
ξ,ε,ω,δ	Angles pertaining to light refraction through FEP, °

Abbreviation

BWR	Boiling Water Reactor
CANDU	Canada Deuterium Uranium
CAMEL	Crossflow Adapted Measurements and Experiments with LDA
CFD	Computational Fluid Dynamics
FEP	Fluorinated Ethylene Propylene
PMMA	Polymethyl Methacrylate
LDA	Laser Doppler Anemometry
LMFR	Liquid Metal Fast Reactor
LES	Large Eddy Simulation
PWR	Pressurized Water Reactor
RIM	Refractive Index Matching
URANS	Unsteady Reynolds-Averaged Navier-Stokes

Subscript

w	Pertaining to water
BULK	Bulk flow region
GAP	Gap flow region
rms	Root mean square
a	Pertaining to air
p	Pertaining to the LDA probe
sp	Pertaining to span-wise component
st	Pertaining to stream-wise component
infl	Stream-wise velocity profile inflection point
min	Lower limit of flow structure lengths
Max	Upper limit of flow structure lengths

and Tavoularis, 2014). Baratto investigated the air flow inside a 5-rod model of a CANDU fuel bundle (Baratto et al., 2006). The frequency of passage of the coherent structures was found to decrease with the gap size, along the circumferential direction. Gosset and Tavoularis (2006), and Piot and Tavoularis (2011) investigated at a fundamental level the lateral mass transfer inside a narrow eccentric annular gap by means of flow visualization techniques. The instability mechanism responsible for cross-flow was found to be dependent on a critical Reynolds number, strongly affected by the geometry of the gap. Parallel numerical efforts have been made by Chang and Tavoularis with URANS (Chang and Tavoularis, 2005) and by Merzari and Ninokata with LES (Merzari and Ninokata, 2011) to reproduce the complex flow inside such a geometry. However, the effects that the gap geometry has on cross-flow, and in particular the P/D ratio, has been debated long since and yet, a generally accepted conclusion is still seeked. Moreover detecting lateral flow pulsations is yet an hard task (Xiong et al., 2014).

This work aims to measure cross-flow as well as the effects that Reynolds and P/D have on the size of the structures. Near-wall measurements in water are performed with the non-intrusive LDA measurement system inside small gaps and in the presence of FEP.

2. Experimental setup

The experimental apparatus is composed by the test setup, CAMEL, and by the Laser Doppler Anemometry system. The water enters the facility from two inlets at the bottom and flows inside the lateral subchannels and through the gap in between. The outlets are located at the top and the water is collected in an upper vessel. The flow rate is manually adjusted by two valves at the inlet lines and monitored by two pairs of magnetic flow-meters (for inlet and outlet lines). At the measurement section, one of the two half-rods is made of FEP (Fig. 1). A scheme of the loop is pictured in Fig. 2 FEP is a Refractive Index Matching material since it has the same refractive index of water at 20 °C (η_{FEP} = 1.338 (Mahmood et al., 2011); η_w = 1.333 (Tilton and Taylor, 1938) with 532 nm wavelength); it can be employed to minimise the refraction of the laser light. To reduce the distortion of light even more, the FEP half-rod is filled with water. The spacing between the rods can

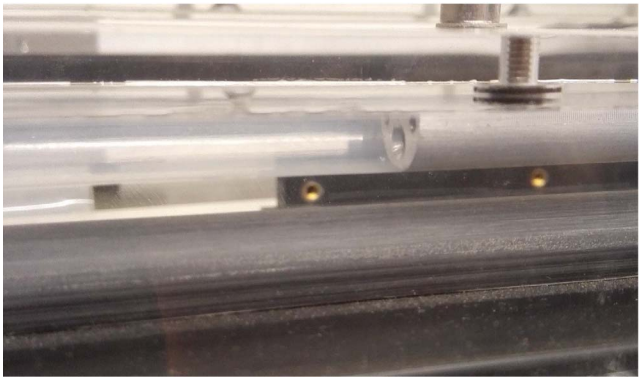

Fig. 1. Hollow half-rod of FEP seen from the outside of the transparent test section: of the two half-rods the top grey one is the rod hosting the FEP section.

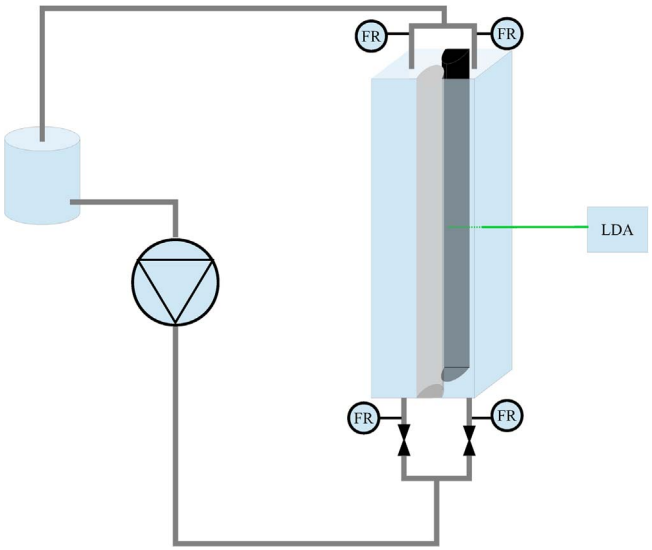

Fig. 2. CAMEL test loop: the flow is provided by a centrifugal pump, it is regulated by 2 manual valves at the inlet branches and is monitored by 4 magnetic flow-recorders (FR). The water flows out from the top of the test section and it is collected inside a vessel.

be adjusted to P/D ratios of 1.07, 1.13 and 1.2. The measured quantities are the stream-wise and span-wise velocity components and their fluctuations. The dimensions of the test section are reported in Table 1.

2.1. CAMEL test setup

The test section is a rectangular Perspex box with two half-rods installed in front of each other (Fig. 1).

2.2. LDA equipment

The measurement system is a 2-components LDA system from DANTEC: a green laser beam pair ($\lambda = 532$ nm) measures the stream-wise velocity component and a yellow laser beam pair ($\lambda = 561$ nm) the lateral component with a maximum power of 300 mW. The measurement settings are chosen through the BSA Flow Software from DANTEC. The flow is seeded with particles to scatter the light and allow the detection in the probe volume. Borosilicate glass hollow spheres with an average density of 1.1 $\frac{g}{cm^3}$ and a diameter of 9–13 μm are employed. In each beam pair one laser has the frequency shifted to detect also the direction of motion of the particle. The LDA is moved by a traverse system and, to provide a dark background, the whole apparatus is enclosed by a black curtain.

2.2.1. Uncertainty quantification

The measurements are provided with a 95% confidence level. Their evaluation has different expressions for mean velocities and root mean square values. They are

$$\varepsilon_m = \frac{U_{rms}}{\overline{U}\sqrt{N_s}} \quad \varepsilon_{rms} = \frac{1}{\sqrt{2N_s}} \tag{1}$$

where ε_m and ε_{rms} are the 95% confidence intervals for mean values and root mean square of the velocity components, U_{rms} is the root mean square of a velocity component, $\overline{U}$ is the mean velocity and N_s is the number of collected samples.

Each measurements point has been measured for a time window long enough to achieve sufficiently narrow confidence intervals. At high flow rates the recording time has been set to 30 s whereas, for low flow rates, the recording time was set as long as 120 s.

ε_{rms} is determined by the number of collected samples only. The most critical conditions are encountered at very low Reynolds numbers and in the centre of the gap because the laser beams must pass the FEP half-rod (see path A, Fig. 3). Here, the maximum ε_{rms} is 1.5%.

ε_m depends also on the mean velocity value $\overline{U}$ as well, thus the requirement are even more strict than for ε_{rms}. The lower the Reynolds number, the more samples are required. With a P/D of 1.2 (i.e. 3 mm gap spacing, see Table 1), for example, $\varepsilon_m = 0.8\%$ for the stream-wise component and becomes $\varepsilon_m = 0.5\%$ when measuring from the side (path B). The span-wise velocity exhibits even more significant uncertainties since it is always characterised by near-zero values. ε_m increases when the measurement volume approaches the wall (lower data rate) and when the gap width is reduced (reflection of light, see Fig. 3). In the latter case, the issue of the light reflected into the photodetector can be tackled to some extent (see Section 7.3).

2.3. Experimental campaign

The measurements are taken on two lines: along the symmetry line of the gap, from one sub-channel to the other, and at the centre of the gap along the rod-to-rod direction. For each P/D ratio different flow rates are considered such that different Reynolds numbers are established. The first series of measurements is done with the laser going through the FEP half-rod (Fig. 3) and by mapping the symmetry line through the gap.The second series of experiments is done with the light entering the setup through the short Perspex side (Fig. 4) without crossing the FEP; in the latter case the measurements are taken along both the symmetry line through the gap and normal to the rods at the centre. The Reynolds number of the bulk flow, Re_{BULK}, is calculated using the stream-wise velocity at the centre of the sub-channels as follows:

$$Re_{BULK} = \frac{\rho_w \cdot V_{BULK} \cdot D_H}{\mu_w} \tag{2}$$

where ρ_w is the water density, μ_w is the water dynamic viscosity, V_{BULK} is the stream-wise bulk velocity calculated as $V_{BULK=\frac{\dot{V}}{A}}$ where $\dot{V}$ is the total flow rate and A is the total flow area, $D_H \equiv \frac{4A}{P_H}$ is the hydraulic diameter of the test section, being P_H the wetted perimeter. The Reynolds number of the gap, Re_{GAP}, is calculated as:

$$Re_{GAP} = \frac{\rho_w \cdot v_{GAP} \cdot D_{H,GAP}}{\mu_w} \tag{3}$$

where $D_{H,GAP}$ is the gap hydraulic diameter defined by the flow area bounded by the two half-rod walls and closed by the gap borders at the rod ends.

v_{GAP} is the average stream-wise velocity through the gap region: the velocity profile is measured over the area A shown in Fig. 5. The average stream-wise gap velocity v_{GAP} is calculated as:

$$v_{GAP} = \frac{1}{A}\int_{z_1}^{z_2}\int_{x_1}^{x_2} v_y(x,z)\,dx\,dz \tag{4}$$

Table 1
CAMEL main dimensions. R_{rod}: half-rod diameter, L: Perspex boxlong side, H: Perspex box short side, t_{PMMA}: Perspex wall thickness, t_{FEP}: FEP half-rod wall thickness, W: gap spacing.

Quantity		Value [mm]
R_{rod}		7.5
L		58.2
H		26
t_{PMMA}		8
t_{FEP}		0.3
W	P/D = 1.07	1
	P/D = 1.13	2
	P/D = 1.20	3

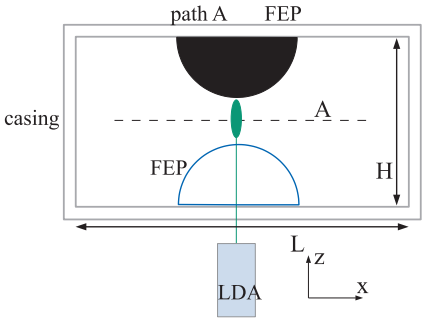

Fig. 3. Top view of the measurement crossing the FEP. The ellipsoidal measurement volume is represented as well; the solid green line represents the laser beam (Figure not drawn to scale).

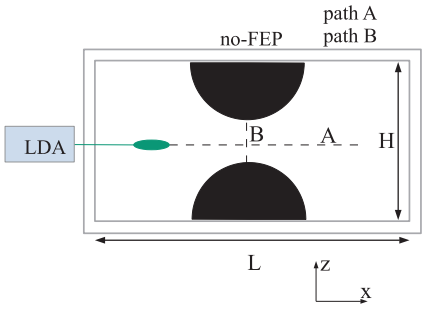

Fig. 4. Top view of the measurement without crossing the FEP. The measurement paths are the dashed lines.

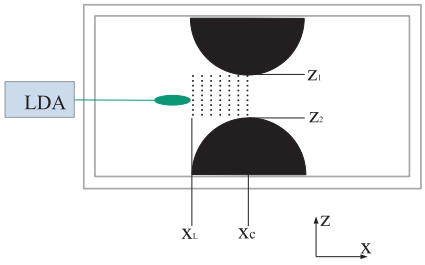

Fig. 5. Top view of the flow area over which the gap Reynolds number is estimated.

Table 2
Test matrix of the experiments. Each value of the flow rate corresponds to a Reynolds number of the main sub-channel (Re_{BULK}). The Reynolds number of the gap (Re_{GAP}) is measured for the three P/D ratios.

$\dot{V}$ [l/s]	Re_{BULK}	Exp. Re_{GAP}		
P/D =		1.07	1.13	1.20
0.96	29,000	3000	3800	5000
0.68	20,000	2160	2750	3400
0.38	12,000	1100	1500	1760
0.22	6500	580	880	930
0.12	3600	310	400	600
0.08	2400	130	200	470
0.04	1200	100	100	190
0.02	600	30	50	130

where x_1,x_2,z_1,z_2 are the coordinates defining the area A. Flow rate, Re_{BULK} and Re_{GAP} for the three P/D ratios are reported in Table 2.

3. Stream-wise RMS along the GAP (path A; no-FEP)

The stream-wise velocity component v and its root mean square v_{rms} are measured along path A (no-FEP) (Figs. 6 and 4). The data are then corrected for the refraction of light through the Perspex wall (see 7.1). The measurements are normalised by the bulk velocity calculated as $\dot{V}/A$. The two main sub-channels are located at $|X/D| = 1$, where the stream-wise velocity profile reaches the highest value. The centre of the gap is at $X/D = 0$, where the minimum occurs. The relative difference between the velocity in the bulk and in the gap becomes more evident if either the Reynolds or the P/D decrease. Fig. 7 compares the results obtained with the present geometry and the geometry used by Mahmood at similar Reynolds numbers (Mahmood et al., 2011). The relative velocity difference between the bulk region and the gap centre is larger in the two half-rods geometry (squares) than in the one consisting of only one half-rod, especially at a low flow rate. The v_{rms} profile shown in the following figure corresponds to a P/D of 1.07; the horizontal coordinate is normalised to the half-rod diameter. The v_{rms} profile of Fig. 8 presents two peaks at the borders of the gap (X/D = ±0.5) and a dip in the centre. As the measurement approaches the walls of the Perspex encasing ($|X/D| > 1$) the v_{rms} increases like in common wall-bounded flows. The water enters the facility from the bottom via two bent rubber pipes next to each other leading to an unwanted non-zero lateral momentum transfer among the sub-channels. This results in the asymmetry of the v_{rms} profile visible at the borders of the gap in Fig. 8. At lower flow rates the v_{rms} is symmetric with respect to the gap centre (Fig. 9). With P/D of 1.13 and 1.2 the profile is found to be symmetric at all the investigated flow rates (Fig. 10). Flow oscillations are damped by the gap region (Gosset and Tavoularis, 2006), especially for smaller gaps where the confinement of lateral momentum within the sub-channel is more dominant. If the gap size is increased, such transversal components may redistribute among the sub-channels and this can be the reason of the symmetric v_{rms} profile. The v_{rms} profiles are shown in Figs. 8 and 9. Due to the refraction of the laser light through the Perspex wall (see Section 7.1) the measurement positions could be corrected by using Eq. 20. Nevertheless, due to Perspex thickness tolerance (10% of the nominal thickness t_{PMMA}) and the spatial resolution of the measurement volume a slight asymmetry remains in the plots.

4. Stream-wise RMS normal to the walls (path B; no-FEP)

The wall-normal stream-wise velocity component and its root mean square v_{rms} are measured at the centre of the gap for each P/D ratio with different flow rates along path-B (no-FEP) (Figs. 11–13). The results for each Re_{BULK} are measured along the centreline between the two rods, from wall to wall. The velocity profile changes from fully turbulent at Re_{BULK} = 29,000 to laminar with Re_{BULK} = 2400. The flow shows some analogy with common channel flows since the v_{rms} has two near-wall peaks where the viscous stresses equal the Reynolds shear stresses (Pope, 2000) and the turbulent production reaches a maximum. A dip occurs in the centre (Fig. 12, Re_{BULK} = 29,000, 20,000 and 12,000). v_{rms} decreases closer to the walls due to the effect of the viscous sub-layer: velocity fluctuations can still occur inside this region but they are caused by turbulent transport from the log-layer region (Nieuwstadt et al., 2016). With the Re_{BULK} of 12,000 and P/D of 1.07 a weak third peak in the v_{rms} appears between the rod walls. As Re_{BULK} is decreased to 6500, this additional peak becomes clearer and dominant over the near-wall peaks. The v_{rms} with P/D of 1.13 and 1.2 do not display such a peak as Re_{BULK} is decreased from 29,000 to 6500, although the near-wall peaks become less sharp. The v_{rms} measured at lower Re_{BULK} is shown in Fig. 13. The v_{rms} measured with Re_{BULK} of 3600 increases towards the centre for P/D of 1.07 and 1.13 whereas the v_{rms} with P/D of 1.2 still displays a weak dip there. If Re_{BULK} is further decreased to 2400 the three P/D ratios have the same increasing trend towards the centre. With Re_{BULK} of 1200 and 600 the different P/D ratios cause major differences in the corresponding v_{rms} profile. The central v_{rms} peak can be originated by the transport of turbulence from the borders (where the production is higher) towards the centre by means of cross-flow. This hypothesis could be in agreement with previous numerical and experimental works (Chang and Tavoularis, 2005Guellouz and

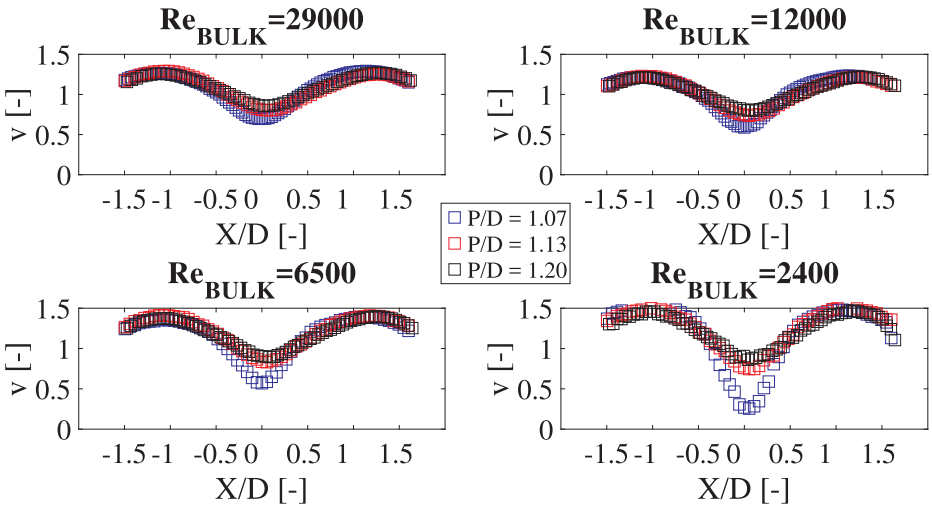

Fig. 6. Stream-wise velocity component against the normalised horizontal coordinate along the gap for Re_{BULK} of 29,000, 12,000, 6500 and 2400. The data are normalised by the bulk velocity.

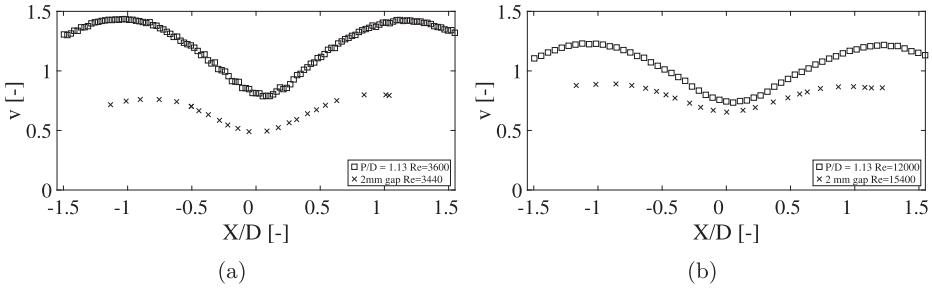

Fig. 7. Comparison between the stream-wise velocity profile with P/D = 1.13 (2 mm gap spacing) and experiments from Mahmood et al. (2011). 7(a): stream-wise velocity normalised by the bulk velocity at Re_{BULK} = 3600 compared with data obtained at Re = 3440. 7(b): stream-wise velocity normalised by the bulk velocity at Re_{BULK} = 12,000 compared with data obtained at Re = 15,400. Data from Mahmood et al. (2011) are measured with a similar geometry consisting of one half-rod.

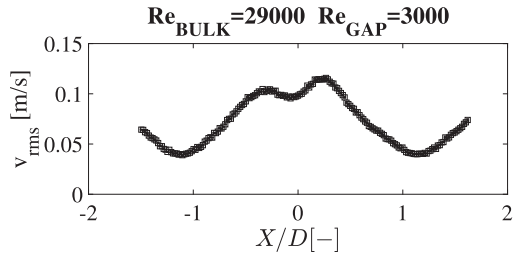

Fig. 8. v_{rms} profile along the gap; P/D = 1.07. The asymmetry is due to the lateral momentum component of the flow in the main sub-channels.

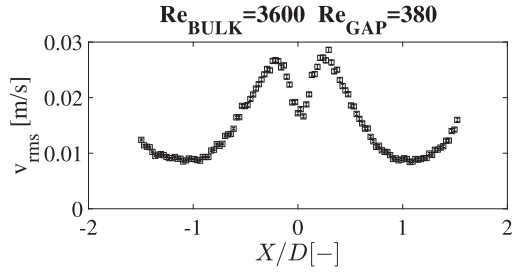

Fig. 9. v_{rms} profile along the gap; P/D = 1.07. As the flow rate is decreased, the effects of the lateral momentum component disappear.

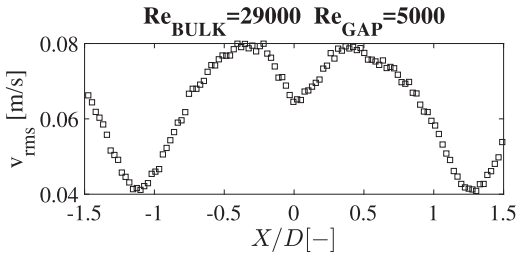

Fig. 10. v_{rms} profile along the gap; P/D = 1.2. The profile looks symmetric even with the highest flow rate: the larger gap, here, allows the lateral momentum component of the flow to redistribute between the two sub-channels.

Tavoularis, 2000Merzari and Ninokata, 2011). An analogous additional peak in the root mean square has been found in the middle of the gap, which is attributed to the lateral passage of structures. Moreover, another numerical work by Merzari and Ninokata highlighted that such structures grow in importance as the Reynolds number decreases. For a Reynolds of 27,100 they are found to be missing, whereas with Re = 12,000 they become more dominant in the flow field (Merzari and Ninokata, 2009).

5. Velocity profile normal to the walls

In this section an hypothesis about the physical meaning of the central peak measured in the v_{rms} profile (Section 4) will be tested: the assumption is that this peak is caused by the two near-wall v_{rms} maxima which migrate towards the centre of the gap as Re_{BULK} is decreased, close enough to merge. In a very small channel, like the gaps studied here, the two near-wall v_{rms} peaks, by approaching each other, could merge together to form the central peak observed in Figs. 12 and 13. The reasoning behind this assumption is described and then it will be experimentally investigated by comparing the velocity profile and the v_{rms} profile normal to the half-rods (path B; no-FEP). In wall-bounded flows, if Re decreases, the viscous wall region extends towards the centre of the channel (Pope, 2000). This would imply that the two near-wall peaks in the v_{rms} profile move closer to each other. The buffer layer is usually the region where the near-wall peak in the v_{rms} occurs because most of the turbulent production takes place here (Nieuwstadt et al., 2016). In the hypothesis that the central v_{rms} peak is produced by the two merging near-wall v_{rms} maxima, the buffer layer should also extend to the central part of the gap channel. The analysis of the velocity profile normal to the half-rod walls (path B, no-FEP), plotted against the

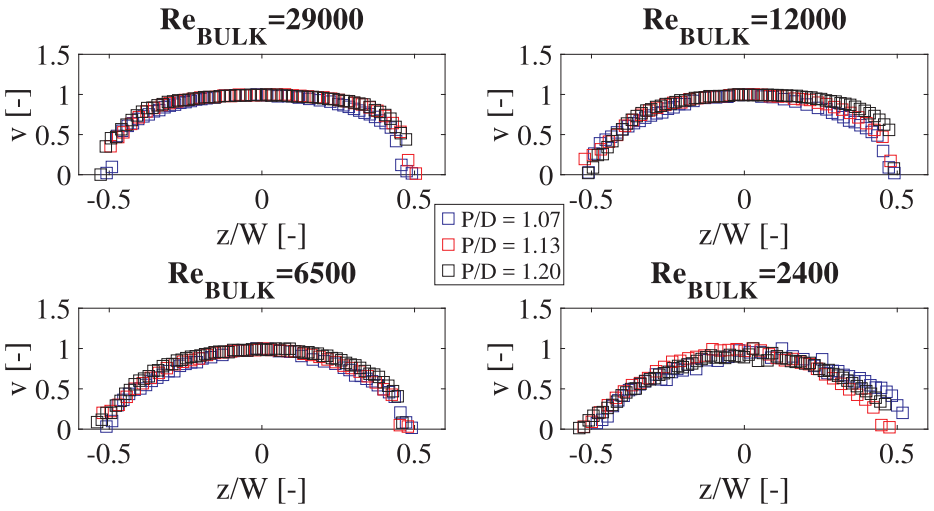

Fig. 11. Stream-wise velocity component against the normalised wall-normal coordinate at the centre of the gap for Re_{BULK} of 29,000, 12,000, 6500 and 2400. The data are normalised by the velocity in the centre at $z/W = 0$.

non dimensional wall distance z^+, helps to verify whether or not the buffer layer actually grows in extension enough to move the near-wall v_{rms} peaks close enough to merge. The following plots show both the velocity profile and the v_{rms} normal to the half-rod walls (line B, no-FEP; Fig. 4). The results along path B are represented with a pair of plots for each measurement. The top one refers to the half of the gap spanning from the centre to the Rod 1 wall ($z^+ = 0$); likewise the bottom one involves the Rod 2 wall ($z^+ = 0$). Fig. 14 refers to P/D = 1.07 with Re_{BULK} = 12,000, which corresponds to the highest flow rate where the central v_{rms} peak is found. It shows two near-wall v_{rms} peaks ($z^+ = 11$) and a flat plateau in the centre of the gap channel. The near-wall peaks are clearly located within the buffer layer (i.e. where the velocity profile changes from linear to logarithmic) close to each half-rod wall. Fig. 15 shows that with P/D = 1.07 and a lower Re_{BULK} of 6500 the central dominant peak of the v_{rms} profile cannot be caused by the near-wall maxima merging together: the two buffer regions are located close to the respective half-rod walls, which proves that the consequent near-wall peaks have not migrated towards the centre of the gap. When the flow rate is further decreased to Re_{BULK} = 3600, only one broad peak in the v_{rms} profile is present at the centre of the gap (Fig. 16); nonetheless the (weak) transition between linear and logarithmic velocity profile, which individuates the buffer layer, can still be located far from the centre of the gap channel. At lower Reynolds values the buffer layer cannot be found anymore because of the laminarization of the flow inside the gap.

Fig. 17 refers to an higher P/D ration, i.e. P/D = 1.13 and Re_{BULK} = 6500. The v_{rms} profile presents two near-wall relative maxima ($z^+ = 40$) corresponding to the location of the buffer layers; a dominant plateau in the v_{rms} profile is found to occupy the centre of the gap channel outside the buffer regions. The above findings discard the hypothesis of the central v_{rms} peak as a result of the union of the two near-wall maxima since the buffer layers remain close to the walls, far apart from being merged. Therefore a second hypothesis is investigated: the central v_{rms} peak at the centre of the gap can be originated by cross-flow pulsations of coherent structures moving from one sub-channel to the other, across the gap. The signature of their passage, therefore, is searched in the span-wise velocity component data series, which will be described in the next section. The analysis of the frequency spectrum of the span-wise velocity component can clarify this assumption: the periodical lateral flow would appear as a peak in the spectrum (Möller, 1991; Baratto et al., 2006).

6. Autocorrelation analysis

The study of the autocorrelation function and of the frequency spectrum of the span-wise velocity is a powerful method to determine if a periodical behaviour is present in the flow. The spectrum is computed with Matlab from the autocorrelation of the span-wise velocity component.

The statistical characteristics of a signal can be determined by computing the ensemble average (i.e. time average, for stationary conditions) (Tavoularis, 2005). However, this is not possible with the

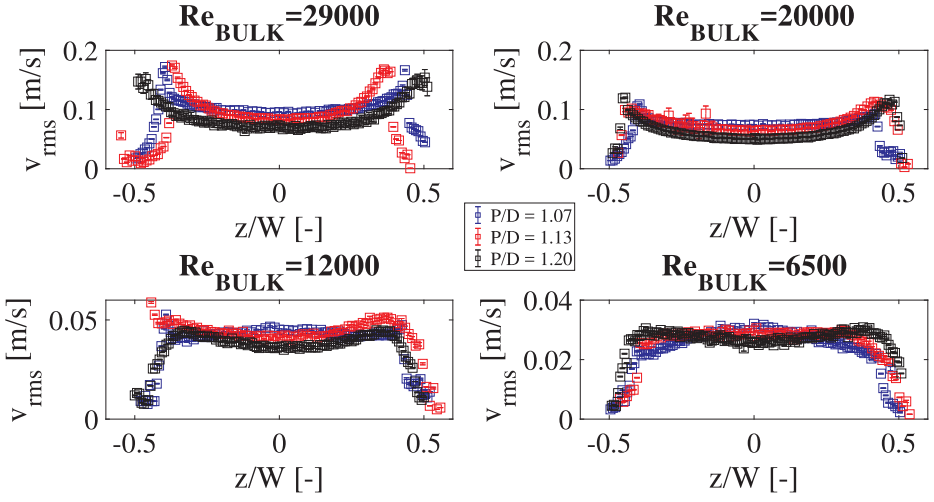

Fig. 12. v_{rms} at the centre of the gap (path B; no-FEP), between the half-rod walls; the measurements are taken with Re_{BULK} = 29,000, Re_{BULK} = 20,000, Re_{BULK} = 12,000 and Re_{BULK} = 6500 with P/D ratio of 1.2 (black), 1.13 (red) and 1.07 (blue). As Re decreases, a weak peak appears first with P/D = 1.07 (Re_{BULK} = 12,000) and it also interests also P/D = 1.13 at lower flow rate (Re_{BULK} = 6500). (For interpretation of the references to colour in this figure legend, the reader is referred to the web version of this article.)

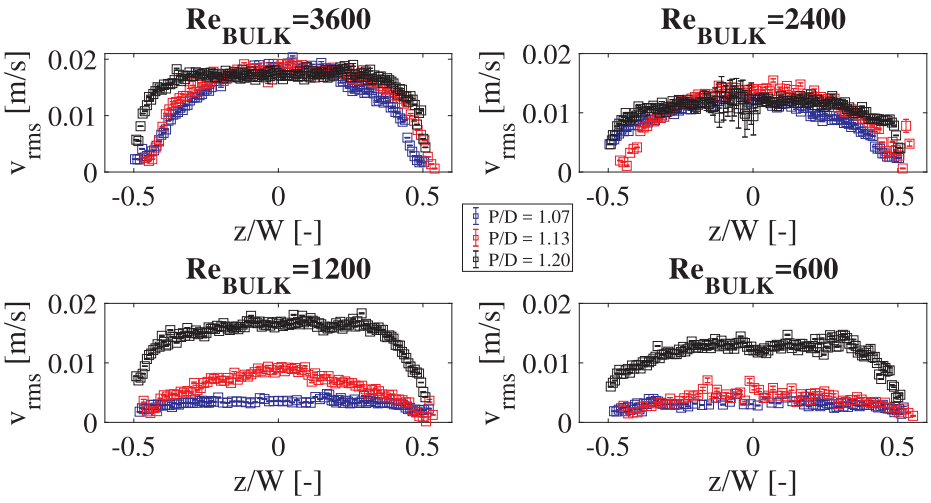

Fig. 13. v_{rms} at the centre of the gap (path B; no-FEP), between the half-rod walls; the measurements are taken with Re_{BULK} = 3600, Re_{BULK} = 2400, Re_{BULK} = 1200 and Re_{BULK} = 600 with P/D ratio of 1.2 (black), 1.13 (red) and 1.07 (blue). As the Re is further decreased (Re_{BULK} = 3600, 2400), the P/D = 1.2 also leads to an increase of turbulence between the rod walls, in the centre of the gap. (For interpretation of the references to colour in this figure legend, the reader is referred to the web version of this article.)

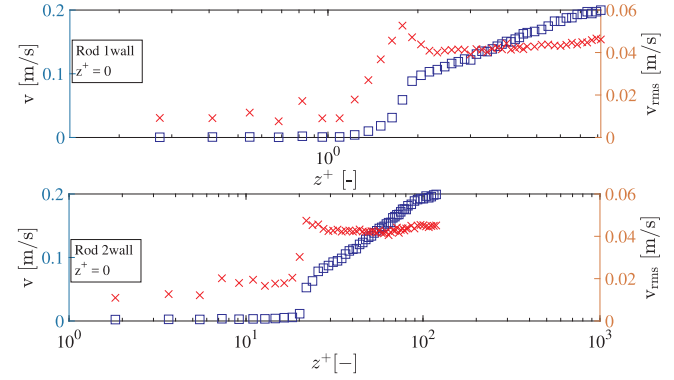

Fig. 14. Stream-wise velocity profile (blue) and v_{rms} (red). P/D = 1.07, Re_{BULK} = 12,000, Re_{GAP} = 1100. The v_{rms} peak is located within the buffer layer of the velocity profile. (For interpretation of the references to colour in this figure legend, the reader is referred to the web version of this article.)

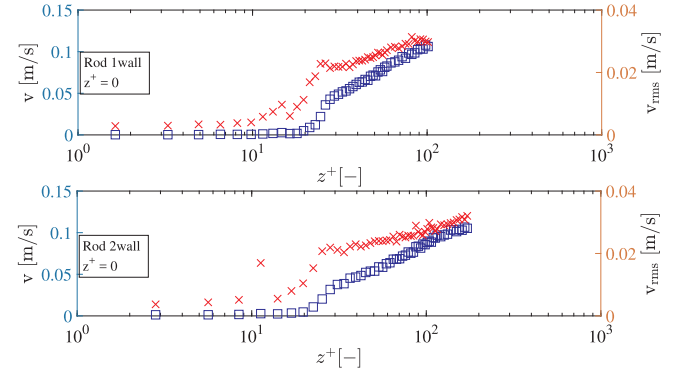

Fig. 15. Stream-wise velocity profile (blue) and v_{rms} (red). P/D = 1.07, Re_{BULK} = 6500, Re_{GAP} = 580. Although a central v_{rms} peak is present, this is not caused by the near-wall peaks; they are still close to the respective walls, within the buffer layer. (For interpretation of the references to colour in this figure legend, the reader is referred to the web version of this article.)

output signal of the LDA system due to the randomness of the sampling process (i.e. the samples are not evenly spaced in time). The slotting technique is the alternative method used here.

6.1. The slotting technique

Sample pairs with inter-arrival time falling within a certain time interval (lag time) are allocated into the same time *slot*. Then the ensemble average is calculated, in each slot, by computing the cross-product of the sample velocities of each pair (Mayo, 1974; Tummers and Passchier, 2001; Tummers et al., 1996). The effect of the (uncorrelated) noise, embedded within the velocity signal, is evident when the first point of the autocorrelation function is evaluated at zero lag time: here the autocorrelation would present a discontinuity and the spectrum would be biased by the noise at high frequencies. The slotting technique omits the self-products from the estimation of the autocorrelation function. The effect of the noise bias, which are strong in the centre of the gap, are reduced.

6.1.1. Velocity bias

Generally the spectrum can also be biased towards higher velocities (i.e. higher frequencies) since the amount of high speed particles going through the measurement volume is larger than the one for low speed particles (Adrian and Yao, 1986). Consequently their contribution to the spectrum will be higher than the real one. The slotting technique used in this work adopts the transit time weighting algorithm to weight the velocity samples with their residence time within the measurement probe. This diminishes the velocity bias influence on the spectrum, especially with high data rate.

6.1.2. Spectrum variance

The randomness of the sampling process contributes in increasing the variance of the spectrum, which can be reduced by increasing the mean seeding data rate through the probe. However, this is not always possible, especially in regions with very low velocity such as the centre of the gap. Consequently, the so-called Fuzzy algorithm is used. Cross-products with inter-arrival time closer to the centre of a slot will, thus, contribute more to the autocorrelation estimation (Nobach, 2015; Nobach, 1999).

6.2. Cross-flow pulsations

The span-wise velocity is measured across the (path A, FEP) FEP half-rod (see Fig. 3). The spectrum is calculated at each measurement point from the bulk of the left sub-channel to the centre of the gap, for all the studied flow rates and P/D ratios. A peak in the spectrum appears for Re_{BULK} below 6500 and at different measurement points close to the centre. The frequency spectrum with Re_{BULK} of 6500 and a P/D of 1.07 at three locations near the gap centre is shown in Fig. 18. The peak in the power spectra proves that the span-wise velocity component of the flow near the centre of the gap oscillates in time with a low frequency. This frequency corresponds to the abscissa of the spectrum peak reported in the plot. This behaviour can be induced by large coherent flow structures near the borders that periodically cross the gap.

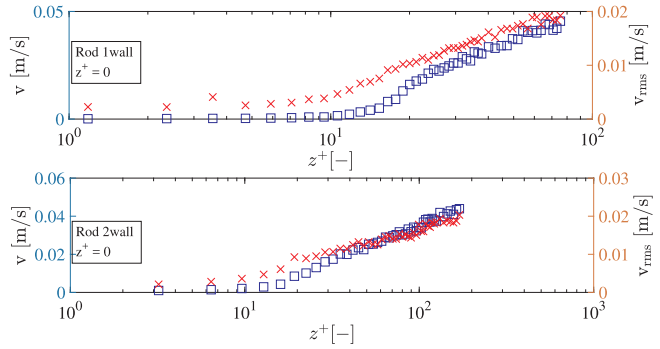

Fig. 16. Stream-wise velocity profile (blue) and v_{rms} (red). P/D = 1.07, Re_{BULK} = 3600, Re_{GAP} = 310. A broad v_{rms} peak occurs in the centre of the gap. The buffer layers, and the corresponding v_{rms} peaks, are still located close to the rod walls, not being the cause of the central increase of turbulence. (For interpretation of the references to colour in this figure legend, the reader is referred to the web version of this article.)

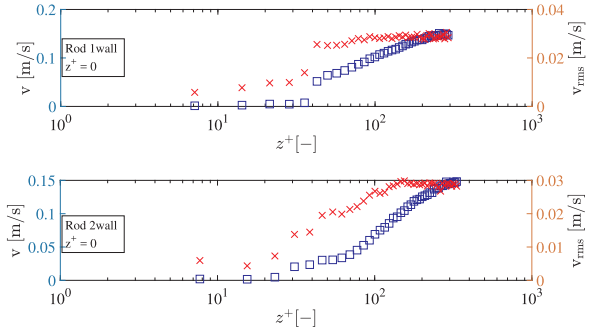

Fig. 17. Stream-wise velocity profile (blue) and v_{rms} (red). P/D = 1.13, Re_{BULK} = 6500, Re_{GAP} = 880. The v_{rms} profile features a central plauteau which is not caused by the two near-wall peaks. (For interpretation of the references to colour in this figure legend, the reader is referred to the web version of this article.)

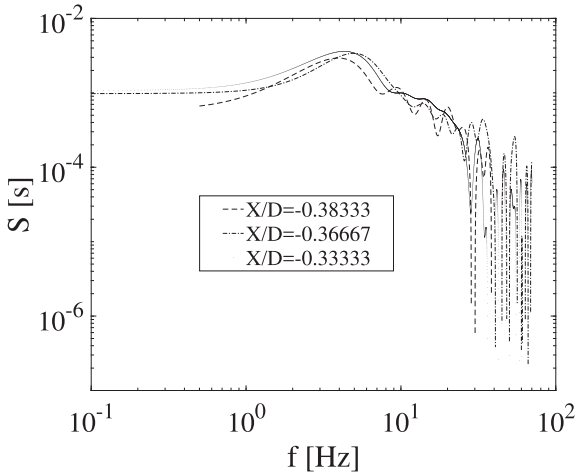

Fig. 18. Spectral estimator of the span-wise velocity component; Re_{BULK} = 6500, P/D = 1.07 for three locations near the centre of the gap (the horizontal coordinate X is normalised to the half-rod diameter D). A peak is evident near 3.8 Hz.

The spectral peak is fitted with a Gaussian bell and the standard deviation σ_{sp} around the mean value is calculated. For each Re_{BULK} and P/D ratio the average frequency is taken and the average standard deviation is used to include also the span-wise frequencies falling within the spectral peak. The following figures show the dependency of the average span-wise frequency of cross-flow of structures on P/D and Re_{BULK}. As for the Re dependency, Fig. 19 shows that the frequency of the span-wise velocity component decreases with Re_{BULK}, and that this occurs for all the P/D ratios. Moreover at Re_{BULK} = 1200, a P/D = 1.07 shows a steep drop in the frequency and at Re_{BULK} of 600 no peak in the spectrum is found; P/D = 1.13 and P/D = 1.2, however, display low frequency behaviour with Re_{BULK} = 600. The values of Fig. 19 are used to express the span-wise frequency in non-dimensional terms. The Strouhal number is thus defined as:

$$Str = \frac{\overline{f}_{sp} \cdot \sqrt{D_{rod} \cdot \mathbf{W}}}{v_{infl}} \tag{5}$$

where $\overline{f}_{sp}$ is the average frequency at which the structures cross the gap, D_{rod} is the half-rod diameter, W is the gap spacing and v_{infl} is the stream-wise velocity at the inflection point ($\frac{\partial^2 v}{\partial x^2} = 0$) of the velocity profile (path A, no-FEP Fig. 4), where the velocity gradient is the largest (Goulart et al., 2014). Fig. 20 confirms only in part what has been observed by Möller (1991), where the Strouhal number was reported to be independent on the Reynolds number and affected only by geometrical parameters. However, at low Reynolds numbers, this trend is maintained only for a P/D = 1.2. P/D = 1.13 and P/D = 1.07, instead, exhibit a decrease in Str as the flow rate is lowered. This asymptotic behaviour of Str for high Re is also found by Choueiri and Tavoularis in their experimental work with an eccentric annular channel (Choueiri and Tavoularis, 2015). Given the importance of two parameters such as the rod diameter D_{rod} and the gap spacing W in rod bundle experiments, the characteristic length scale of the Strouhal number includes both, as shown by Meyer et al. (1995). Our findings and those of Möller are reported in Fig. 21. Note that Möller used a different definition for the Strouhal number, namely

$$Str_\tau = \frac{\overline{f}_{sp} \cdot D_{rod}}{u^*} \tag{6}$$

where u^* is the friction velocity. Fig. 21 confirms that the Strouhal is independent of the Reynolds. However, at very low Re the trend exhibits some variation. As for the P/D dependency, Fig. 22a highlights that for Re_{BULK} of 6500, 3600 and 2400 the frequency of cross-flow decreases with increasing gap spacing. This seems to contradict a precedent work (Baratto et al., 2006) where a different geometry, resembling a CANDU rod bundle, is used. The data from Fig. 22a are reported in Fig. 22b in terms of Strouhal number, defined in Eq. (5). In this Re interval, Str appears to be inversely proportional to the gap spacing W (or to the P/D), as found also by Wu and Trupp (1994). The following correlation is proposed:

$$1/Str = 31.232 \cdot W/D_{rod} + 6.6148 \tag{7}$$

where W is the gap spacing. Eq. (7) describes the overall trend of the experimental points measured for three P/D values in the range $2400 \leqslant Re_{BULK} \leq 6500$. Note that this correlation is an estimation of the overall trend. However, if the data series corresponding to the three P/D ratios are considered separately, the dependence between $1/Str$ and P/D is not necessarily linear.

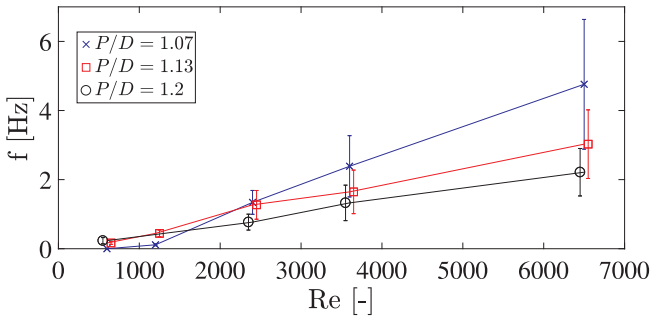

Fig. 19. Average frequency of periodicity in the span-wise velocity component against Re_{BULK} for the three P/D ratios.

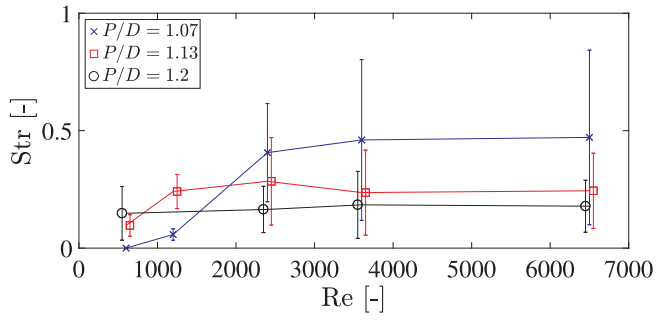

Fig. 20. Average non-dimensional span-wise frequency versus Re_{BULK} for three P/D ratios.

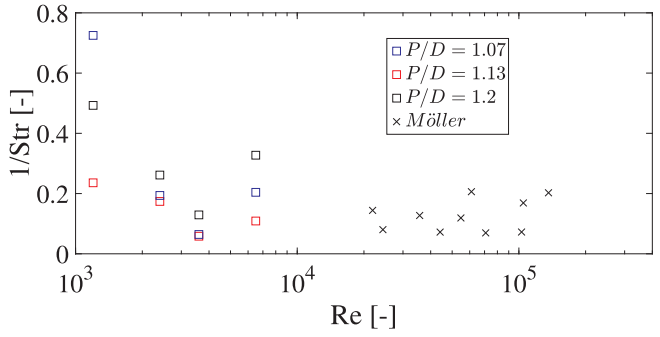

Fig. 21. $1/Str$ against the Reynolds number for the three P/D values compared with Möller (1991).

6.3. Stream-wise gap vortex streets

The stream-wise velocity component has been studied with the same method to calculate the average frequency and the standard deviation of cross-flow pulsations as in the previous section. The stream-wise velocity data series measured at in the left-hand side of the gap (path A, no-FEP Fig. 4) are used to calculate the frequency spectrum. Where a periodical behaviour is confirmed by a peak in the spectrum, the average frequency is plotted at the corresponding location within the gap. By plotting, in the same graph, the value of the frequency and the location where such periodicity is detected, one can have an idea of both the value of the frequency and of the spatial extension of the structures within the flow. The results obtained with the three P/D ratios are reported in the following figures along the normalised horizontal coordinate (gap centre at $X/D = 0$; left gap border at $X/D = -0.5$). A periodical behaviour has been found for all the P/D ratios at different locations within the gap and inside the main sub-channel close to the gap borders, which is characteristic of the presence of gap vortex streets moving along with the stream. Fig. 23 refers to P/D = 1.07. This case shows that the frequency at which the flow structures pass by increases with Re_{BULK}. For $Re_{BULK} = 600$ the periodical flow structures stretch out into the main sub-channel whereas, as the Reynolds increases, they become more localised within the gap. Fig. 24 refers to a larger P/D ratio, i.e. P/D = 1.13. This case shows again that the frequency increases with Re_{BULK} but, differently than with P/D = 1.07, the spatial distribution of points appears more scattered at high Reynolds. This finding indicates that the periodical flow structures generally cover a larger region of the flow, extending from the centre of the gap towards the main sub-channel. The locations where these structures are found tend to move closer to the gap centre as the

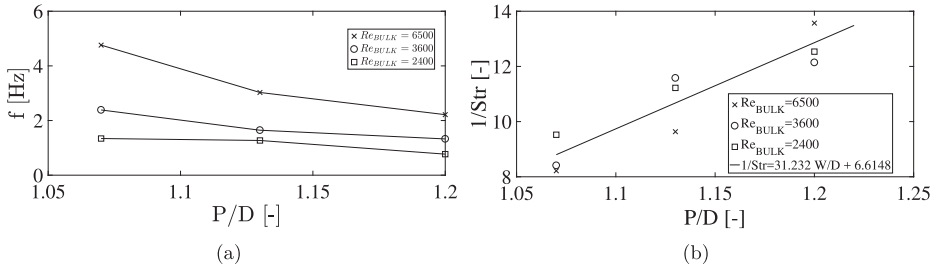

Fig. 22. (a): Average span-wise frequency against P/D for three Re numbers. (b): $1/Str$ against P/D: experimental results and proposed correlation.

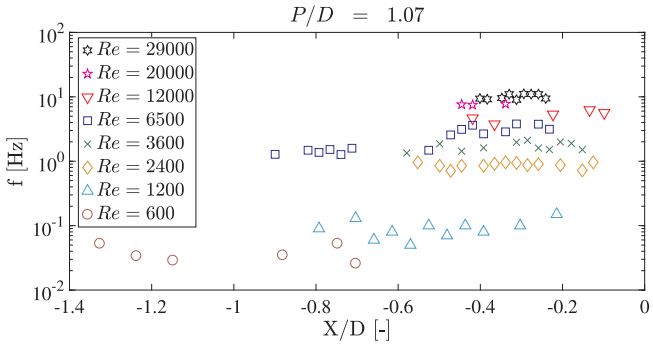

Fig. 23. Average stream-wise frequency of the flow structures and their locations for the investigated Re; P/D = 1.07. As Re_{BULK} increases the structures move further inward into the gap and they appear less scattered.

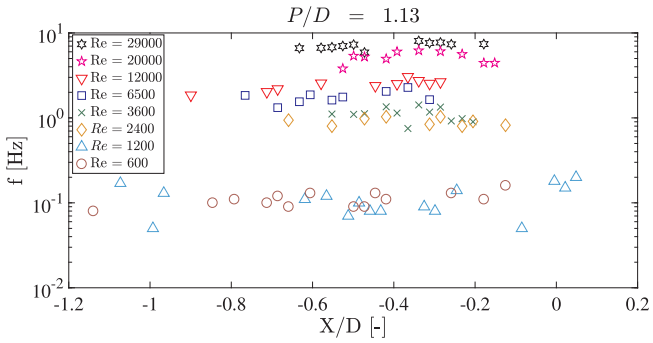

Fig. 24. Average stream-wise frequency of the flow structures and their locations for the investigated Re; P/D = 1.13.

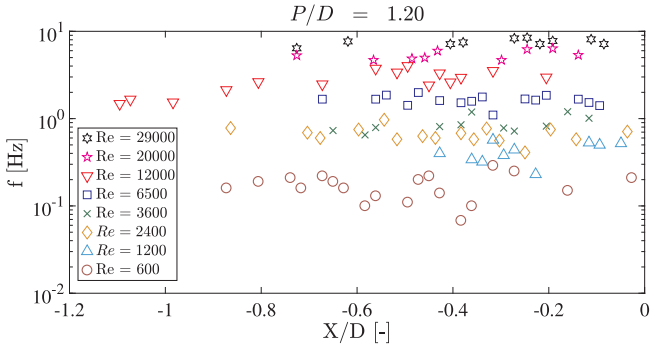

Fig. 25. Average stream-wise frequency of the flow structures and their locations for the investigated Re; P/D = 1.2. Even at high Re_{BULK} the flow structures are detected over a broader region of the gap than with P/D = 1.07 and P/D = 1.13.

Reynolds increases, similarly to what has been observed with P/D = 1.07.

Fig. 25 refers to the largest P/D ratio, i.e. P/D = 1.2. This case leads to periodical flow structures spread over the gap and the main channel even more than smaller P/D ratios; as Re_{BULK} increases the structures do not exhibit the tendency to move toward the centre of the gap.

The adoption of the Taylor's hypothesis (i.e. assuming the vortices as frozen bodies carried by the main flow) enables to estimate the average length of the vortices, moving in trains along the stream-wise direction. Although this assumption may become inaccurate with very long structures (Marusic et al., 2010), experiments in bundles show that these vortices move with a convection velocity which is independent of the position inside the gap (Meyer, 2010). The structure length is calculated as:

$$\mathscr{L} = \frac{v_{infl}}{\overline{f}_{st}} \tag{8}$$

where $\overline{f}_{st}$ is the average frequency at which the structures pass by the measurement volume and v_{infl} is their stream-wise convection velocity taken at the inflection point of the velocity profile through the gap (path A, no-FEP Fig. 4). The non dimensional stream-wise frequency is expressed in terms of Strouhal number, as presented in Section 6.2. Similarly to the span-wise frequency, the Strouhal number shows an asymptotic trend at high flow rates (Fig. 26), whereas it presents a strong dependency on the Reynolds number when the flow rate decreases. The standard deviation σ_{st} around the average stream-wise frequency is used to calculate the lower and upper limit around the mean structure length

$$\mathscr{L}_{\min} = \frac{v_{infl}}{\overline{f}_{st} + \sigma_{st}} \quad \mathscr{L}_{\mathrm{Max}} = \frac{v_{infl}}{\overline{f}_{st} - \sigma_{st}} \tag{9}$$

The average, minimum and maximum stream-wise lengths of the coherent structures are shown for each considered Re_{BULK} in the following figure. As for Re dependency, the periodical structures become longer with decreasing Re_{BULK}; this is in agreement with the findings of Mahmood et al. (2011) and Lexmond et al. (2005) for compound channels. With increasing Re_{BULK}, the stream-wise length tends to reach an asymptotic value, as observed by Gosset and Tavoularis (2006). As for geometry dependency, an increasing P/D (i.e. larger gap spacing) causes the structures to lengthen; this is observed within the range $2400 \leqslant Re_{BULK} \leq 29{,}000$. At lower Reynolds values this tendency appears to be reversed. From Fig. 27 it appears that with $Re_{BULK} \geqslant 2400$ the length of the periodical structures is merely affected by geometrical parameters such as the gap spacing; this confirms what has been stated by Meyer et al. (1995) for compound rectangular channels and by Guellouz and Tavoularis (2000) for a rectangular channel with one rod. However, for $Re_{BULK} \leq 2400$ Re_{BULK} has a strong influence on the stream-wise structure size are evident. According to Kolmogorov's length scale, tha ratio between the largest and smallest vortices, d_{Max} and d_{min} respectively, is proportional to $Re^{3/4}$ (Kolmogorov, 1962). Assuming that, for $Re_{BULK} \geqslant 2400$, the scale of the large flow structures is constant

$$[d_{min} \cdot Re^{3/4}]_{\mathrm{Re}=2400} = [d_{min} \cdot Re^{3/4}]_{\mathrm{Re}=29{,}000} \tag{10}$$

The Kolmogorov microscale d_{min} is given by $\nu^{3/4} \cdot \varepsilon_d^{-1/4}$ where ν is the kinematic viscosity and ε_d is the energy dissipation rate. Eq. (10) gives

$$[\nu^{3/4} \cdot \varepsilon_{\mathrm{d}}^{-1/4} \cdot Re^{3/4}]_{Re=2400} = [\nu^{3/4} \cdot \varepsilon_{\mathrm{d}}^{-1/4} \cdot Re^{3/4}]_{Re=29{,}000} \tag{11}$$

which leads to the more general form

$$\frac{Re^3}{\varepsilon_{\mathrm{d}}} = cost. \tag{12}$$

From Eq. (12) it follows that the dissipation rate at the largest considered Reynolds number is 1750 times higher than the dissipation rate at $Re_{BULK} = 2400$.

The lengthening of the structures at low flow rates (Fig. 27), and the widening of the range where they are found (Figs. 23–25) seem to indicate that coherent structures grow both in length and in width as the Reynolds is decreased.

7. Parameters affecting the experiment

The v_{rms} measured along path A for the FEP and no-FEP cases (see Figs. 3 and 4) are compared to study the effects of the light refraction and reflection.

7.1. Light refraction

In one case (Fig. 3) the refraction occurs when the laser crosses the FEP rod and in the other case (Fig. 4) it is caused by the Perspex wall as the probe volume moves further inside the test section. Both cases have been corrected for the refraction. The half beam angles through the Perspex wall β and in water γ (Fig. 29) are calculated. Referring to Fig. 28

$$\sin\delta = \mathrm{x}/R_i \tag{13}$$

where δ is the angle of incidence of the light ray with respect to the normal to the half-rod inner wall, $R_i = 7.2$ mm is the inner radius of FEP and x is the lateral distance from the centre of the rod.

$$\sin\varepsilon = \sin\delta \frac{\eta_w}{\eta_{FEP}} \tag{14}$$

where ϵ is the angle of the refracted light ray through the FEP and $\eta_{FEP} = 1.338$ is the FEP refractive index (Mahmood et al., 2011). Considering the triangle AOB and applying the law of sine twice

$$\begin{cases} \frac{\mathrm{AB}}{\sin\omega} = \frac{R_i}{\sin\xi} \\ \frac{\mathrm{AB}}{\sin\omega} = \frac{R_i + t_{FEP}}{\sin(180° - \varepsilon)} \end{cases} \tag{15}$$

Hence,

$$\sin\gamma = \sin\varepsilon \frac{R_i}{R_i + t_{FEP}} \tag{16}$$

$$\omega = 180° - \gamma + \varepsilon \tag{17}$$

Applying the law of cosine to the triangle AOB

$$\mathrm{AB}^2 = R_i^2 + (R_i + t_{FEP})^2 - 2R_i(R_i + t_{FEP})\cos\omega \tag{18}$$

The horizontal distortion of the light ray due to the presence of FEP is

$$\Delta\,\mathrm{x} = \mathrm{AB}\sin(\delta - \varepsilon) \tag{19}$$

Considering Fig. 29, the position of the probe volume inside the setup, corrected by the refraction due to the Perspex wall, is given by

$$\mathrm{X(x)} = \frac{x_0 - t_{PMMA}\tan\beta}{\tan\gamma} - \frac{L}{2} \tag{20}$$

where x_0 is the position of the probe volume without refraction, t_{PMMA} is

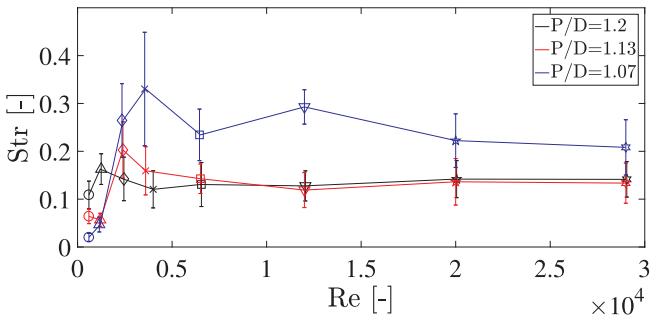

Fig. 26. Average non-dimensional stream-wise frequency versus Re_{BULK} for three P/D ratios. A strong dependency on the Re appears at low values of Re_{BULK}.

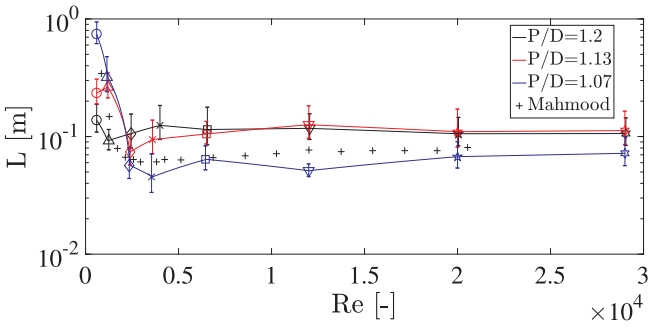

Fig. 27. Stream-wise coherent structures length versus Re_{BULK} for three P/D ratios. The experiments are compared with data from Mahmood et al. (2011). The length of the flow structures tends to an asymptotic value as Re_{BULK} increases, whereas they become longer at low flow rates.

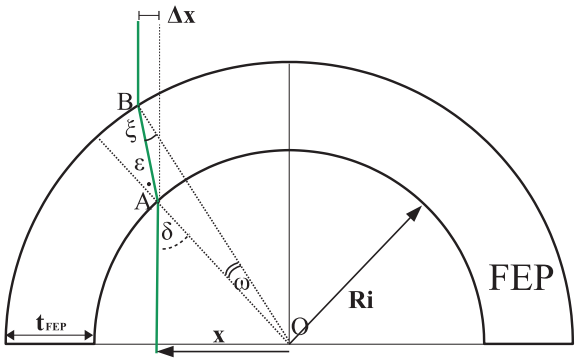

Fig. 28. Top view of the refraction of the green laser beam pair due to FEP. the light ray goes through the FEP half-rod, filled with water, and it is refracted as it crosses its wall. The refraction Δx can be calculated by geometrical considerations.

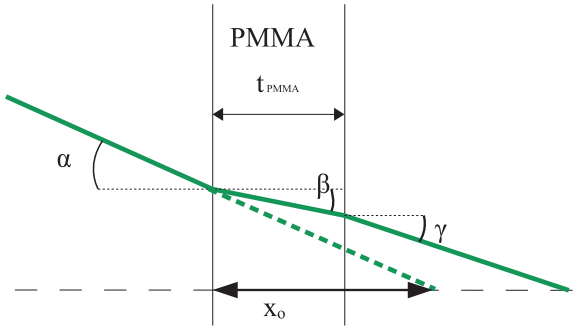

Fig. 29. Refraction of the green laser beam pair due to the Perspex wall. For reason of symmetry with respect to the horizontal, only one laser beam is represented. α: LDA half-beam angle, β: angle of the light through the Perspex, γ: angle of the light in water (obtained by applying the law of Snell). The light ray arrives at the outer Perspex wall inclined by half-beam angle α and it is refracted twice, through the wall and inside the water.

the Perspex wall thickness and L is the length of the long side of the Perspex encasing box (see Table 1).

Eqs. (19) and (20) are applied to the measured series of data. The v_{rms} measured through the FEP half-rod (path A, FEP) and from the short side (path A, no-FEP) are shown in the following figure. (Fig. 30).

The two v_{rms} profiles are still slightly shifted with respect to each other after the refraction correction is applied: Eq. (19) and (20) depend on t_{PMMA},t_{FEP} and on R_i which vary due to the dimensional tolerance of the material. This introduces a source of uncertainty in the refraction calculation. Moreover, when the laser reaches the FEP borders (X/ D= ±0.5), the light is not transmitted anymore and the signal drops to zero.

7.2. Probe volume length

The refraction of the laser beam pair affects the size of the probe volume as well (Chang et al., 2014). The length of its long axis, in air, can be calculated by

$$l_{p,a} = \frac{d_0}{\sin\alpha} = 0.9 \text{ mm} \quad (21)$$

where d_0 is the laser beam diameter at the focal point, as given by Guenther (1990). Applying the same relation but using the half-beam angle in water γ (see Fig. 29) the axis length is

$$l_{p,w} = \frac{d_0}{\sin\gamma} = 1.2 \text{ mm} \quad (22)$$

If the measurement is taken in the case of FEP (see Fig. 3), the probe volume is oriented with the long axis normal to the rods. The increased length of the probe makes it more difficult to fit in the centre of the gap when the spacing is adjusted to 1 mm (P/D = 1.07); this implies also an increased reflection of light from the rod wall. The v_{rms} measured with the laser light going through the FEP and from the free side of the setup (red and blue data set respectively in the following plots) are compared to assess the influence of the elongated ellipsoidal probe volume. The v_{rms} of Figs. 31 and 32 refer to P/D = 1.07. Fig. 31 shows that the v_{rms} measured through the FEP rod is peaked at the centre of the gap. The light reflected by the rod behind the probe volume is registered as seeding particles with near-zero velocity next to the velocity given by the real samples. The effect is the peak in the v_{rms} (which is a measure of the deviation around the mean velocity) in the centre, where reflection is strong and the probe volume touches the walls. The v_{rms} profiles measured at lower flow rates are shown in Fig. 32. The v_{rms} measured through the FEP rod does not show the central peak found at higher Re. Although the light reflection and the elongated probe volume still contribute with near-zero velocity signals, the v_{rms} is not peaked because the flow velocity closer to zero reduces the statistical deviation. Fig. 33 refers to the case with P/D = 1.2 (gap spacing of 3 mm). With a larger gap, the reflection becomes weaker and the probe fits the gap well. The quality of the results improves as shown in Fig. 33 where the two v_{rms} match.

7.3. Light reflection

When measuring along path A in case of FEP (see Fig. 3) the measurement is affected by light reflection from the second rod which is behind the ellipsoidal measurement volume. As the probe is moved further towards the centre of the gap the reflection becomes important, especially for the P/D of 1.07. The problem of the light reflected into the photo-detector from the wall behind the measurement volume can be tackled by filtering out the near-zero velocity contribution. This

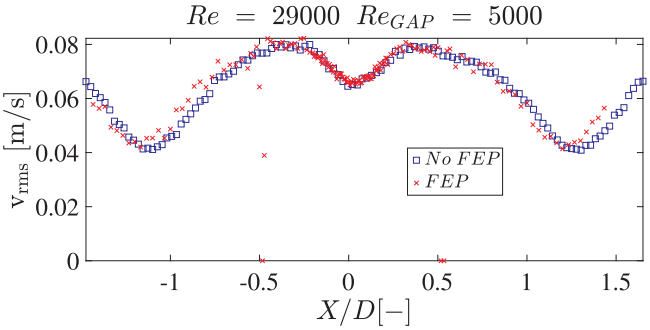

Fig. 30. v_{rms} against the position along the gap normalized to the rod diameter: comparison between refracted and corrected results. Path A, FEP (red series) and path A, no-FEP (blue series). Rod borders at $|X/D| \leq 0.5$, P/D = 1.2. (For interpretation of the references to colour in this figure legend, the reader is referred to the web version of this article.)

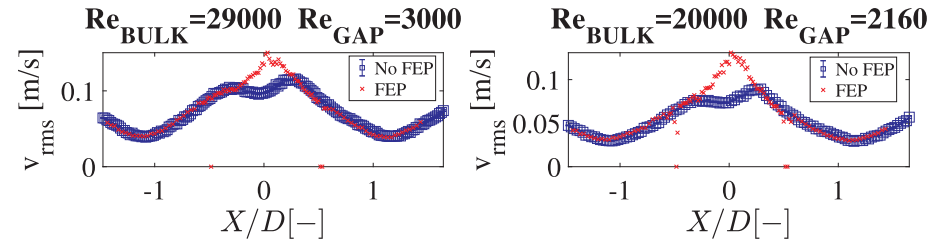

Fig. 31. Measurement of v_{rms} along path A FEP (red series) and along path A no-FEP from the second side (blue series); P/D = 1.07. The effect of a too small gap, compared to the probe size, is the central peak due to reflection of light and contact between the masurement volume and the walls; it is interpreted by the software as zero-velocity signal. (For interpretation of the references to colour in this figure legend, the reader is referred to the web version of this article.)

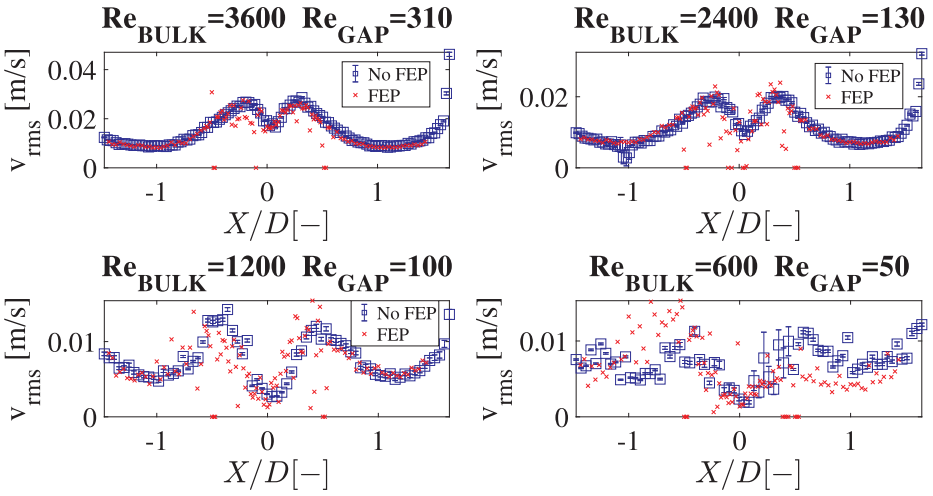

Fig. 32. v_{rms} along the gap through the FEP (red series) and from the second side (blue series); P/D = 1.07. (For interpretation of the references to colour in this figure legend, the reader is referred to the web version of this article.)

improves the results as long as the ellipsoidal volume fits the gap and the flow speed is not too close to zero. The cases where the filter was successfully applied are shown in Fig. 34. In Fig. 34(a) the filtered v_{rms} yet shows some dispersion close to the left border of the gap (X/D = −0.5). The filtered v_{rms} shows an improvement at the measurement points where the raw data show some degree of scattering. It occurs because FEP has the highest light attenuation as the borders of the rod are approached: here the laser path inside FEP is much longer. The data rate drops sensibly and the lower number of recorded samples exhibits wider fluctuations.

8. Conclusions

The flow between two rods in a square channel has been measured with three P/D ratios and channel Reynolds numbers. As the flow rate decreases, an additional peak in the root mean square of the stream-

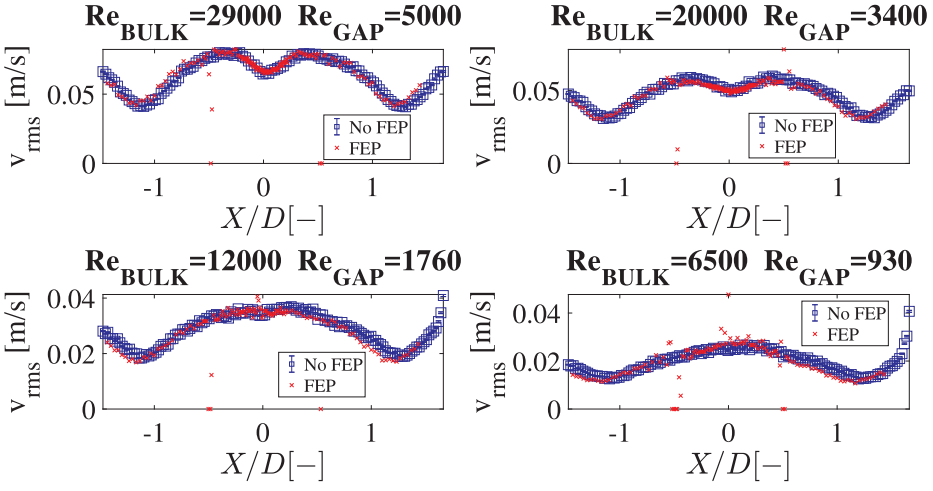

Fig. 33. v_{rms} along the gap through the FEP (red series) and from the second side (blue series); P/D = 1.2. The measurement probe volume fits well the larger gap and it allows for a correct measurement of the v_{rms}. (For interpretation of the references to colour in this figure legend, the reader is referred to the web version of this article.)

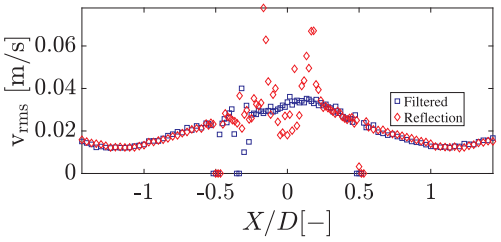

(a) P/D=1.13.

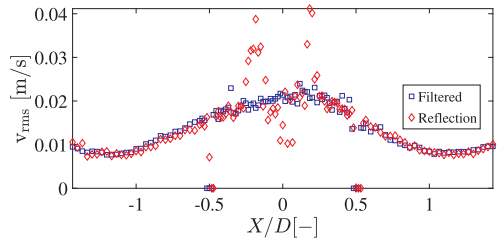

(b) P/D=1.13.

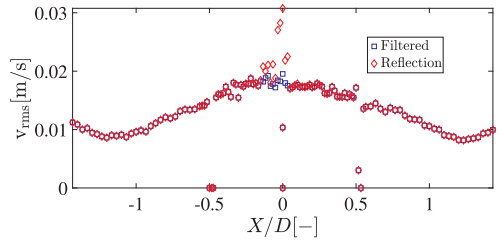

(c) P/D=1.2.

Fig. 34. Comparison between the v_{rms} affected by light reflection from the wall (red) and filtered (blue). The reflection can be corrected with a filter on the measured velocity provided this is sufficiently higher than zero. (a): Re_{BULK} = 6500, Re_{GAP} = 880; (b): Re_{BULK} = 3600, Re_{GAP} = 400; (c): Re_{BULK} = 3600, Re_{GAP} = 600. (For interpretation of the references to colour in this figure legend, the reader is referred to the web version of this article.)

wise velocity is found at the centre of the gap; it becomes clearer and occurs at higher Re as the gap spacing is reduced. The occurrence of the peak can be related to the presence of coherent structures across the gap which increase cross-flow. The power spectrum of the span-wise velocity exhibits a peak near the gap centre revealing the presence of such periodical structures in the transversal direction. The frequency of cross-flow decreases with Re. The study of the stream-wise velocity component highlights the presence of coherent structures near the gap border; their length is affected by the geometry and by the Reynolds only when the latter reaches low values. Moreover, as Re is decreased, these structures are found also further away from the border into the main sub-channel; this points out that coherent structures may grow not only in length, but also in width if Re decreases. When the laser beam enters the setup it is refracted leading to an elongation of the LDA probe volume. This intensifies the light reflection when measuring through the FEP normal to the rods, especially in the middle of the gap. With P/D of 1.2 and 1.13 reflection can be filtered out, whereas a P/D of 1.07 leads to biased measurements in the centre since the LDA probe comes in contact with the rod walls. Moreover, FEP performs well while laser goes through it and reflection of light can be tackled as long as the probe volume fits the gap spacing, that is the case of P/D = 1.13 and P/D = 1.2. This study provides an experimental benchmark for validating innovative numerical approaches that have the main goal of reproducing the complex fluid dynamics inside the core of liquid metal reactors.

Future studies to investigate if the present findings depend not only on the P/D ratio, but also on the half-rod diameter, are encouraged.

Acknowledgements

This project has received funding from the Euratom Research and Training Programme 2014–2018 under the grant agreement No. 654935.

The author would like to thank Ing. Dick de Haas and Ing. John Vlieland for the technical support provided during the work.

References

Adrian, R.J., Yao, C.S., 1986. Power spectra of fluid velocities measured by laser Doppler velocimetry. Exp. Fluids 5 (1), 17–28 ISSN 07234864.

Baratto, F., Bailey, S.C.C., Tavoularis, S., 2006. Measurements of frequencies and spatial correlations of coherent structures in rod bundle flows. Nucl. Eng. Des. 236 (17), 1830–1837 ISSN 00295493.

Chang, D., Tavoularis, S., 2005. Unsteady numerical simulations of turbulence and coherent structures in axial flow near a narrow gap. J. Fluids Eng. 127 (3), 458 ISSN 00982202.

Chang, Seok-Kyu, Kim, Seok, Song, Chul-Hwa, 2014. Turbulent mixing in a rod bundle with vaned spacer grids: OECD/NEA-KAERI CFD benchmark exercise test. Nucl. Eng. Des. 279, 19–36 ISSN 00295493.

Choueiri, G.H., Tavoularis, S., 2014. Experimental investigation of flow development and gap vortex street in an eccentric annular channel. Part 1. Overview of the flow structure. J. Fluid Mech. 752 (2014), 521–542 ISSN 0022-1120.

Choueiri, G.H., Tavoularis, S., 2015. Experimental investigation of flow development and gap vortex street in an eccentric annular channel. Part 2. Effects of inlet conditions, diameter ratio, eccentricity and Reynolds number. J. Fluid Mech. 768 (2015), 294–315 ISSN 0022-1120.

Gosset, A., Tavoularis, S., 2006. Laminar flow instability in a rectangular channel with a cylindrical core. Phys. Fluids 18 (4) ISSN 10706631.

Goulart, J., Noleto, L., Sérgio Möller, V., 2014. Experimental study of mixing layer in a closed compound channel. J. Braz. Soc. Mech. Sci. Eng. 36 (2), 411–420 ISSN 1678-5878.

Guellouz, M.S., Tavoularis, S., 2000. The structure of turbulent flow in a rectangular channel containing a cylindrical rod – Part 1: Reynolds-averaged measurements. Exp. Thermal Fluid Sci. 23 (1–2), 59–73 ISSN 08941777.

Guenther, R.D., 1990. Modern Optics. Whiley-VCH.

Kolmogorov, A.N., 1962. A refinement of previous hypotheses concerning the local structure of turbulence. J. Fluid Mech. 13 (September), 83–85 ISSN 0022-1120.

Lexmond, A.S., Mudde, R.F., Van Der Hagen, T.H.J.J., 2005. Visualisation of the vortex street and characterisation of the cross flow in the gap between two sub-channels. In: 11th International Topical Meeting on Nuclear Reactor Thermal-Hydraulics.

Mahmood, A., 2011. Single-Phase Crossflow Mixing in a Vertical Tube Bundle Geometry – An Experimental Study (Ph.D. thesis). Delft University of Technology.

Marusic, I., McKeon, B.J., Monkewitz, P.A., Nagib, H.M., Smits, A.J., Sreenivasan, K.R., 2010. Wall-bounded turbulent flows at high Reynolds numbers: recent advances and key issues. Phys. Fluids 22 (6), 1–24 ISSN 10706631.

Mayo, W.T., 1974. A discussion of limitations and extensions of power spectrum estimation with burst counter LDV Systems. In: Proceedings of the Second International Workshop on Laser Velocimetry, vol. 1. pp 90–101.

Merzari, E., Ninokata, H., 2009. Anisotropic turbulence and coherent structures in eccentric annular channels. Flow Turbul. Combust. 82 (1), 93–120 ISSN 13866184.

Merzari, E., Ninokata, H., 2011. Proper orthogonal decomposition of the flow in a tight lattice rod-bundle. Nucl. Eng. Des. 241 (11), 4621–4632 ISSN 00295493.

Meyer, L., 2010. From discovery to recognition of periodic large scale vortices in rod bundles as source of natural mixing between subchannels – a review. Nucl. Eng. Des. 240 (6), 1575–1588 ISSN 00295493.

Meyer, L., Rehmen, K., 1995. Periodic vortices in flow through channels with longitudinal slots or fins, Tenth Symposioum on Turbulent shear flows, page 6.

Möller, S.V., 1991. On phenomena of turbulent flow through rod bundles. Exp. Thermal Fluid Sci. 4 (1), 25–35 ISSN 08941777.

Nieuwstadt, F.T.M., Boersma, B.J., Westerweel, J., 2016. Turbulence – Introduction to Theory and Applications of Turbulent Flows. Springer Nature.

Nobach, Holger, 1999. Processing of stochastic sampled data in laser Doppler anemometry. In: Proc. 3rd Int. Workshop on Sampling Theory and Applications. pp. 149–154.

Nobach, H., 2015. Fuzzy time quantization and local normalization for the direct spectral estimation from laser Doppler velocimetry data. Exp. Fluids 56 (5), 1–4 ISSN 07234864.

Piot, E., Tavoularis, S., 2011. Gap instability of laminar flows in eccentric annular channels. Nucl. Eng. Des. 241 (11), 4615–4620 ISSN 00295493.

Pope, S.B., 2000. Turbulent Flows. Cambridge University Press, Cambridge (UK).

Rayleigh, Lord, 1879. On the stability, or instability, of certain fluid motions. Proc. London Math. Soc. s1–11 (1), 57–72.

Rehme, K., 1987. The structure of turbulent flow through rod bundles. Nucl. Eng. Des. 99 (C), 141–154 ISSN 00295493.

Rowe, D.S., Johnson, B.M., Knudsen, J.G., 1974. Implications concerning rod bundle crossflow mixing based on measurements of turbulent flow structure. Int. J. Heat Mass Transfer 17 (3), 407–419 ISSN 00179310.

Tavoularis, S., 2005. Measurement in Fluid Mechanics. Cambridge University Press, Cambridge (UK).
Tavoularis, S., 2011. Reprint of: rod bundle vortex networks, gap vortex streets, and gap instability: a nomenclature and some comments on available methodologies. Nucl. Eng. Des. 241 (11), 4612–4614 ISSN 00295493.
Tilton, L.W., Taylor, J.K., 1938. Refractive index and dispersion of distilled water for visible radiation, at temperatures 0 to 60 °c. J. Res. Natl. Bureau Stand. 20, 419–477.
Tummers, M.J., Passchier, D.M., 2001. Spectral analysis of biased LDA data. Meas. Sci. Technol. 12 (10), 1641–1650 ISSN 0957-0233.
Tummers, M.J., Passchier, D.M., 1996. Spectral analysis of individual realization lda data. (Technical report) Delft University of Technology, Faculty of Aerospace Engineering, Report LR 808.
Wu, X., Trupp, A.C., 1994. Spectral measurements and mixing correlation in simulated rod bundle subchannels. Int. J. Heat Mass Transfer 37 (8), 1277–1281 ISSN 00179310.
Xiong, J., Yu, Y., Yu, N., Fu, X., Wang, H., Cheng, X., Yang, Y., 2014. Laser Doppler measurement and CFD validation in 3 x 3 bundle flow. Nucl. Eng. Des. 270, 396–403 ISSN 00295493.